ACS Sustainable Chemistry & Engineering

Research Article

pubs.acs.org/journal/ascecg

Striving Toward Visible Light Photocatalytic Water Splitting Based on Natural Silicate Clay Mineral: The Interface Modification of Attapulgite at the Atomic-Molecular Level

Jian Zhang,[†] Aishi Chen,[†] Lianhui Wang,[†] Xing'ao Li,*[,†] and Wei Huang*[,†,‡]

[†]Key Laboratory for Organic Electronics and Information Displays & Institute of Advanced Materials (IAM), Jiangsu National Synergetic Innovation Center for Advanced Materials (SICAM), Nanjing University of Posts & Telecommunications, Nanjing 210023, P. R. China

[‡]Key Laboratory of Flexible Electronics (KLOFE) & Institute of Advanced Materials (IAM), Jiangsu National Synergetic Innovation Center for Advanced Materials (SICAM), Nanjing Tech University (NanjingTech), Nanjing 211816, P. R. China

ABSTRACT: Development of visible light driven photocatalytic water splitting catalysts for hydrogen production with both high activity and stability has remained a challenge to renewable energy research in the past decades. Herein, for the first time, the interface modified attapulgite (ATP) at the atomic-molecular level was employed as a photocatalyst for hydrogen production from water under visible light illumination. Because of the enhancement of the surface hydroxyl, the increase of dye adsorption, and high efficiency of photoexcited electron injection ability, the maximal hydrogen generation rate over the modified ATP coupled with Eosin Y is 2.9 times higher than that of original ATP, and the highest apparent quantum efficiency reached 28.6% at 490 nm. This work will pave a new pathway for the modification of natural catalysts for visible light driven photocatalytic water splitting technology.

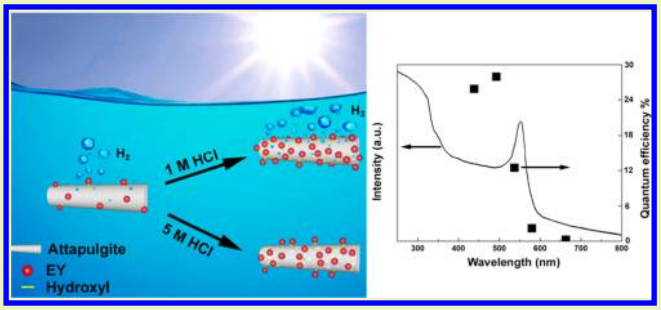

KEYWORDS: *Attapulgite, Interface modification, Water splitting, Hydrogen evolution, Durability*

INTRODUCTION

Photocatalytic production of hydrogen from water using a semiconductor as a photocatalyst is seen to be one of the most promising strategies to meet future energy demands and environmental issues.[1,2] Since the phenomenon was discovered,[3] numerous highly efficient catalysts have been synthesized and investigated for half reactions of water splitting during the past four decades.[4−9] A superior photocatalyst should integrate a suitable conduction band maximum (more negative than the redox potential of H^+/H_2), an appropriate band gap to harvest photons, an enhanced surface reactivity to suppress the photogenerated electron/hole pairs, and durability in water. Considering visible light accounts for approximately 43% of the solar radiation, the development of visible light active photocatalysts is an ambitious mission in this field.[10] Accordingly, a number of visible light responsive photocatalysts for water splitting including oxides,[11−13] sulfides,[14,15] phosphides,[16] and nitrides[17] have attracted more attention in recent years.

Evolution of hydrogen from water by dye sensitization of a semiconductor incorporates some of the principles of natural photosynthetic systems.[18] In general, the basic principle and process of dye-sensitized hydrogen production from water can be described as visible light photon absorption, electron excitation and transformation, and finally photoexcited electron consumption ($2H^+ + 2e \rightarrow H_2$).[19] Considering the short-lived excited state of dye molecules, the primary factor for highly efficient hydrogen production by dye sensitization is strong adsorption of sensitizer molecules onto the surface of a catalyst.[19] Besides, slow electron exchange, low injection quantum yields, and fast electron−hole recombination between photocatalyst and dye molecules may also be important limitations in the system based on dye-sensitized photocatalysis. Understanding the importance of each process requires a detailed kinetic analysis of a dye-sensitized water splitting application.[20]

As a powerful strategy to harvest visible light, Ru(II) polypyridyl sensitizers[21−24] have attracted considerable attention for visible light photocatalytic hydrogen generation from water due to the strong absorption of a fraction of the visible spectrum (below 500 nm), the long-lived lifetime of the excited state (~600 ns), and, most importantly, the participation of almost all excited sensitizer molecules.[25] Recently, Swierk et al. reported an extremely high APCE of 22% under visible light irradiation for transient charge injection from $[Ru(bpy)_2(4,4'\text{-}(PO_3H_2)_2bpy)]$ to the surface of TiO_2.[26] Compared to extensive studies of $Ru(bpy)_3^{2+}$ and its derivatives, metal-free dyes, such as xanthene, melocyanine, and porphine dyes, have

Received: April 8, 2016
Revised: June 14, 2016
Published: July 25, 2016

DOI: 10.1021/acssuschemeng.6b00716
ACS Sustainable Chem. Eng. 2016, 4, 4601−4607

also been investigated with consideration of the low cost as well as high efficiency.[27−29] As a typical organic sensitizer, Eosin Y (EY) dye which sensitizes semiconductors for hydrogen from water under visible light has been under intensive research over 30 years.[30] Besides TiO_2,[31] other active photocatalysts such as ZnO,[32] MoS_2,[33] $Na_2Ti_2O_4(OH)_2$,[34] and Ti-MCM-41[35] sensitized by EY showed relatively excellent photocatalytic activities and long-term stability for hydrogen generation. Motivated by these advances, recently, we focused our interest in dye-[36,37] and quantum-dot[38,39]-sensitized natural Fe-doped silicate clay mineral (attapulgite (ATP) and vermiculite) to effectively split water for hydrogen production under visible light illumination. The highest apparent quantum efficiency (QE) of 10.8% at 483 nm was detected when EY-sensitized ATP was employed as photocatalyst.[36]

Herein, interface modified ATP was prepared through a simple acid treated process with different concentrations. It is shown that the activity of the modified ATP (1 M HCl) is significantly enhanced compared to conventional ATP due to the enhancement of surface hydroxyl, the increase of dye adsorption, and the fast injection of photoexcited electron from EY to ATP. Besides, the photocatalytic system was stable for longer than 15 consecutive days. The findings open up new opportunities for developing an inexpensive and convenient route to split water hydrogen generation from water under visible light.

EXPERIMENTAL SECTION

Preparation of the Modified ATP. All the reagents used in this work were of AR grade obtained from the Shanghai Chemical Factory of China and were used without further purification. ATP was obtained from Xuyi of Jiangsu Province in China. In a typical synthesis of modified ATP, original ATP (0.10 g) was added into the hydrochloric acid solution (20 mL) with different concentration at 50 °C and stirred for 20 h. Then, the precipitate was collected by centrifugation. The resulting products were dried at 60 °C in an air-circulating oven (6 h). Low (1 M) and high (5 M) concentration hydrochloric acid solution treated ATP samples were labeled as LCTATP and HCTATP, respectively.

Characterization. UV−vis absorption spectra of the final products were characterized on a UV3600−NIR-recording spectrophotometer at resolution of 2 nm (Shimadzu, Japan). Fourier transform infrared (FTIR) spectra were collected using a Shimadzu IR Affinity-1 FTIR spectrometer in a range 4000−500 cm^{-1}. Transmission electron microscopy (TEM) and energy dispersive X-ray (EDX, EDAX Genesis 2000) spectroscopy were performed on a JEOL JEM-2100 microscope operating at 200 kV, by depositing a drop of the sample dispersion onto 300 mesh Cu grids coated with a carbon layer. XRD patterns were performed on a BRUKER D8 Advance X-diffractometer (Cu Kα radiation, 1.54056 Å). The photocurrent was measured on an electrochemical system (Chenhua CHI-660D). The visible light was obtained using a 300 W Xe lamp with a 420 nm cutoff filter to completely remove any irradiation below 420 nm.

Dye Absorption Test. In this test, EY was used as an adsorbed dye (4.34×10^{-5} M, 20 mL), which was mixed with the catalysts (20 mg) at room temperature and atmospheric pressure, and the adsorption process was monitored by a UV3600−NIR-recording spectrophotometer (Shimadzu, Japan) at fixed time intervals. The relative concentrations of the EY solution were reflected by the intensity of absorption spectra from the spectrophotometer.

Photocatalytic Tests. The photocatalytic hydrogen production experiments were carried out in a closed gas-circulation system. A 300 W Xe lamp served as the light source, and visible light irradiation was realized by attaching a UV cutoff filter (420 nm). In a typical photocatalytic experiment, 100 mg of catalyst was dispersed in an aqueous solution (100 mL) containing triethanolamine (TEOA) (5%, v/v) as the sacrificial electron donor and EY (0.03 g) as photosensitizer. During irradiation, continuous stirring was applied to keep the samples in suspension (1 h). Evolved hydrogen was analyzed using a gas chromatograph (Shimadzu GC-14C, nitrogen as a carrier gas).

The apparent quantum efficiency (QE) was measured under the same photocatalytic reaction condition. A power meter (1916-R Newport) was used for the measurement of light intensity. The QE values plotted were estimated though several cutoff filters, and were calculated on the basis of the number of the incident photons in each wavelength region. Accordingly, each value is plotted in the middle of two cutoff wavelengths. The QE was calculated according to eq 1:

$$\mathrm{QE}[\%] = \frac{\text{number of reacted electrons}}{\text{number of incident photons}} \times 100 = \frac{\text{number of evolved } H_2 \text{ molecules} \times 2}{\text{number of incident photons}} \times 100 \quad (1)$$

Photoelectrochemical Measurements. Photoelectrochemical performances were evaluated in a three-electrode configuration using an electrochemical workstation (CHI-660D, Shanghai Chenhua, China), a Pt foil as the counter electrode, and Ag/AgCl (saturated KCl) as a reference electrode. A 300 W Xe lamp was used as a light source. Visible light irradiation was realized by attaching a 420 nm cutoff filter. The electrolyte was a mixed solution of 0.35 M Na_2SO_3 and 0.25 M Na_2S (pH = 13.2). After immersion into the EY solution (0.2 M) for 1 h, the slurry was recollected and spread on 1.0×2.0 cm^2 ITO with an active area of 1.0 cm^2 by the doctor blade method. The photoresponses of the electrodes were tested at a constant voltage (0.0 V vs Ag/AgCl). Electrochemical impedance spectroscopy (EIS) measurements were performed at graphite electrodes covered by a deposit of samples (photocatalysts vs EY) in the 0.01−100 000 Hz frequency range, with an application potential of 0.25 V using a 0.35 M Na_2SO_3 and 0.25 M Na_2S as buffer solution.

RESULTS AND DISCUSSION

ATPs are hydrated, porous magnesium aluminum silicate minerals of general formula $(X)_5(Y)_8O_{20}(OH)_2 \cdot 8H_2O$ with ribbon morphology. The "X" (octahedral site) is most commonly occupied by Mg or Al, but can also be occupied by Fe, Ti, or vacancies, while the "Y" (tetrahedral site) is most commonly occupied by Si or Al.[40] Considering the low price, abundance in nature, and nanostructured features, ATPs provide many potential applications such as environmental absorbents, nanocomposites, and catalyst supports.[41−43] In the present study, the interface and crystal structure of ATP were modified through simple acid treatment. As a natural splitting agent, the modified sample ATPs exhibit good photocatalytic activity and are durable coupled with EY under visible light for the water splitting reaction, matching the activity of man-made photocatalysts.[44−46]

XRD profiles for original ATP and different concentration HCl solution treated ATP are shown in Figure 1. The peak positions (2θ) at 8.52°, 19.95°, 27.58°, 35.28°, and 42.76° display the diffraction feature of ATP according to previous research.[47] After treatment with an aqueous solution of HCl (1 M), the primary diffraction peaks of sample LCTATP can be detected which indicates the structure of the ATP is maintained and the interaction occurred on the surface not in the interlayer.[48] It is noticed, however, that the peak intensity of the HCTATP decreases, and even disappears compared to the above two curves. Obviously, amorphous silica can be left with increased concentration of HCl solution (1 M → 5 M) due to the dissolution of octahedral structures (Al−O, Mg−O, and Fe−O) in the crystal of ATP clay.

It is generally accepted that as a typical xanthene dye EY exhibits aggregation effects at high concentrations.[49] From

DOI: 10.1021/acssuschemeng.6b00716
ACS Sustainable Chem. Eng. 2016, 4, 4601−4607

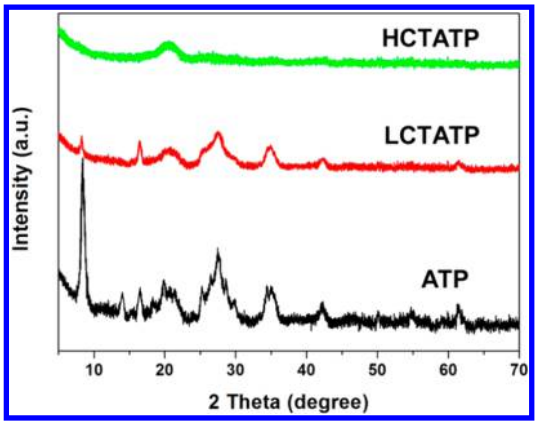

Figure 1. XRD patterns of original ATP and different concentration HCl solution treated ATP (LCTATP, 1 M; HCTATP, 5 M).

Figure 2, a strong peak with maximum at 512 nm with a shoulder at 483 nm can be marked in the absorption spectrum

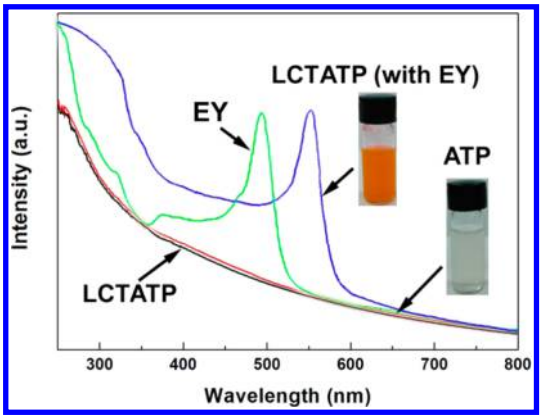

Figure 2. UV−vis absorption spectra of EY aqueous solution (4.34×10^{-5} M), original and modified ATP samples (with and without EY).

of EY (monomer and the dimer (H-type), respectively).[50] The absorption spectrum of original ATP shows strong semiconductor-like behavior in the UV region as well as intrinsic and wide absorption in the visible light region. As the concentration of hydrochloric acid was adjusted to 5 M, LCTATP shows the same absorption feature with original ATP. The absorption peak of the composite of EY and LCTATP is apparently red-shifted to 562 nm compared to that of single EY which implies that some hydrogen bond interactions are constructed between EY molecules and LCTATP.

It is evident that the FTIR spectra are sensitive to slight changes in the octahedral site occupancies in ATP.[51] FTIR spectra of the three samples can generally be separated into three regions as shown in Figure 3. For the typical FTIR spectra of hydrated magnesium aluminum silicate minerals, first, absorption bands in the high frequency region (3700−3200 cm^{-1}) are attributed to the stretch vibrations of structural OH. Second, absorption bands in the middle frequency region (1700−1600 cm^{-1}) are caused by the bend vibration of bound, adsorbed, hygroscopic water or structural OH. Finally, bend vibrations of Si (or Al)−O tetrahedra and M−OH (M = metal element) octahedra are assigned to the low frequency region (900−1200 cm^{-1}).

For the region of high frequency, the band at 3552.2 cm^{-1} is assigned to $(MgFe^{3+})$−OH for the untreated ATP, which is the

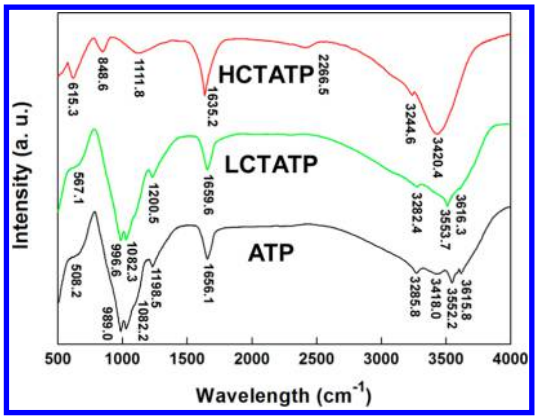

Figure 3. FTIR spectra of ATP, LCTATP, and HCTATP.

primary contribution to the photocatalytic application through constructing a hydrogen bond with EY. After treatment with 1 M HCl, the enhancement of the corresponding band (3535.7 cm^{-1}) and the suppressed shoulder bands (3616.3 cm^{-1} → Al_2−OH, 3417.0 cm^{-1} → Si−OH−Si, and 3282.4 cm^{-1} → Si−(OH)−Al)[51] indicated that the surface hydroxyl of ATP can be selectively activated to enhance the adsorption capacity. With an increase in the concentration of HCl from 1 to 5 M, only Si−OH−Si (3420.4 cm^{-1}) and slight Si−(OH)−Al (3244.6 cm^{-1}) vibrations still exist. In the region of low frequency, the most obvious change of HCTATP is the disappearance of Si−O−M (950−1050 cm^{-1}) (M = Mg, Al, Fe) in a comparison of the three curves. From the above results, we can conclude that the surface of ATP can be selectively activated (the enhancement of $(MgFe^{3+})$−OH) when treated with the low concentration of HCl (1 M) to enhance the adsorption capacity of dye (EY); however, the M−O tetrahedron structure can be destroyed under the concentration of HCl (5 M), resulting in the low efficiency of the photocatalytic system.[52]

To further demonstrate that the interface modification of ATP can increase the adsorption of EY, dye adsorption experiments were carried out at room temperature. As shown in Figure 4, all the samples based on ATP can absorb EY quickly

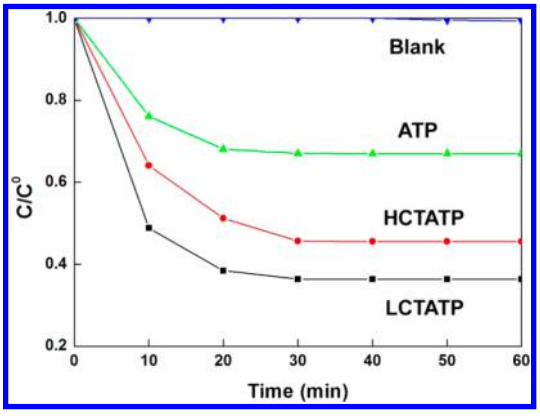

Figure 4. EY adsorption capacity of the samples.

and reach an adsorption balance in 30 min. Notably, sample LCTATP has the best adsorption ability compared to that of the other two samples. The enhanced adsorption ability of LCTATP can be attributed to the selective activation of the ATP surface from a low concentration of HCl solution according to the results from FTIR measurements.

DOI: 10.1021/acssuschemeng.6b00716
ACS Sustainable Chem. Eng. 2016, 4, 4601−4607

TEM and HRTEM images shown in Figure 5a,b confirm the morphology of the original ATP nanorods with a diameter of

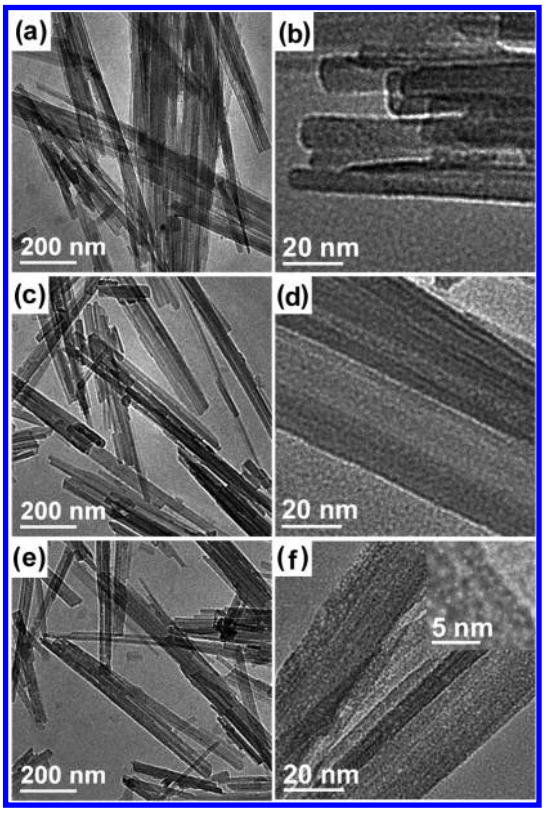

Figure 5. TEM and HRTEM images of the samples (a, b) ATP, (c, d) LCTATP, and (e, f) HCTATP.

20−30 nm and a length of approximately 1 μm. Compared with the original ATP, the morphology of LCTATP has scarcely changed, which indicates that the structure of the ATP is maintained under low concentration HCl solution treated as shown in Figure 5c,d. However, it is interesting to note that the large amounts of micropores can be observed after treatment with high concentration HCl solution, Figure 5e,f. The removal of an M−O (M = metallic elements) tetrahedron from the acid corrosion and the remainder of Si−O octahedron frameworks under 5 M HCl solution correspond to the results of FTIR as well as the XRD measurements.

Figure 6a shows the hydrogen evolution rates of samples with TEOA and EY as sacrificial agents and photosensitizer, respectively, under visible light irradiation. No hydrogen was detected when ATP was used as the photocatalyst without EY because the band gap is too large (3.75 eV)[38] to absorb the visible light. With adsorbed EY as photosensitizer, the activity of sample ATP was remarkably enhanced, and the hydrogen evolution rate was as high as 73 μmol h^{-1}. The dramatic changing of the photocatalysis activity can be observed by comparing the curves LCTATP and HCTATP samples. With treatment with 1 M HCl solution, the hydrogen production rate obtained over the sample LCTATP was further increased to 210 μmol h^{-1}, which is about 2.9 times higher than that of original ATP. The highest activity of photocatalytic hydrogen evolution probably can be attributed to the fact that the increase of dye adsorption[53] of LCTATP and high efficiency of photoexcited electron inject ability from EY to the (MgFe^{3+})−OH group of LCTATP,[36] which is beneficial for visible light

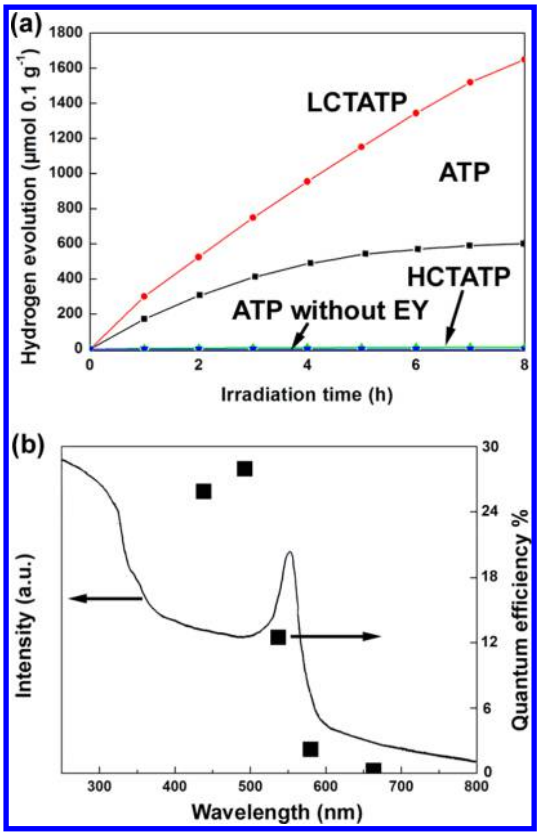

Figure 6. (a) Time course for hydrogen evolution over samples in TEOA (5%, v/v) and EY (0.03 g) mixture solution and (b) influence of wavelength on the apparent QE for hydrogen evolution over LCTATP under visible light irradiation with various wavelengths of 440, 490, 540, 580, and 660 nm.

effective absorption, photogenerated electron injection, and efficient hydrogen evolution. Nevertheless, with the high concentration HCl solution treatment, the HCTATP sample has almost a loss of activity in the same catalytic system (1.3 μmol h^{-1}). It is not difficult to understand the inactivation of HCTATP that just Si−O octahedron frameworks obtained on the basis of the results of XRD and FTIR tests. Figure 6b shows the QE of water splitting by the HCTATP sample coupled with EY as a function of the wavelength of the incident light. The trend of QE matches well with that of absorption in the optical spectra, and the QE reached the highest value of 28.6% at 490 nm, which is almost the highest apparent QE so far reported.[54] Previous results reported the highest QE of 32.5% was reached at 430 nm when EY was used as a photosensitizer for the NiS_x/graphene nanohybrid,[54] but the stability of the materials needs to be further improved (<6 h) compared to our research.

From the viewpoint of practical applications, besides the activity toward the reaction of photocatalysis water splitting, another significant criterion for photocatalyst selection is good durability. Upon the coexistence of TEOA (sacrificial electron donors) and EY (photosensitizer) in the reaction system, the hydrogen evolution of LCTATP catalysts can still retain ca. 92% of the initial hydrogen production rate in the activity over 128 h, as shown in Figure 7. This observed excellent durability of LCTATP should be related not only to the increase of adsorption capacity for EY dye, but also to the inherent stability of the natural silicate clay mineral.

On the basis of the theoretical calculations and chemical analysis, the band gap of ATP has been located from our

DOI: 10.1021/acssuschemeng.6b00716
ACS Sustainable Chem. Eng. 2016, 4, 4601−4607

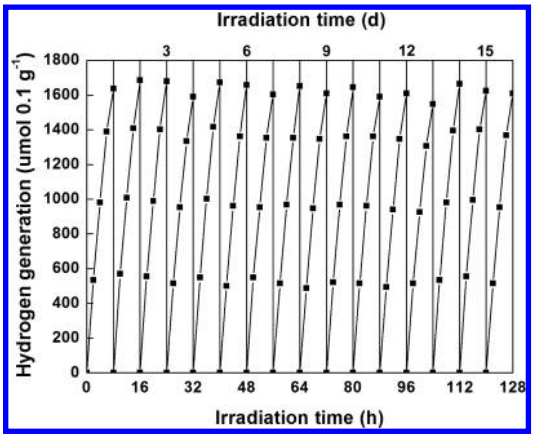

Figure 7. Repeated time course of the photocatalytic hydrogen generation for sample LCTATP under simulated visible light ($\lambda \geq 420$ nm). Experiments were conducted in a 16-day period, with 128 h of the visible light irradiation time.

previous research.[38] In this work, the band structure of the EY-ATP samples is indicated in Figure 8a. Under visible light

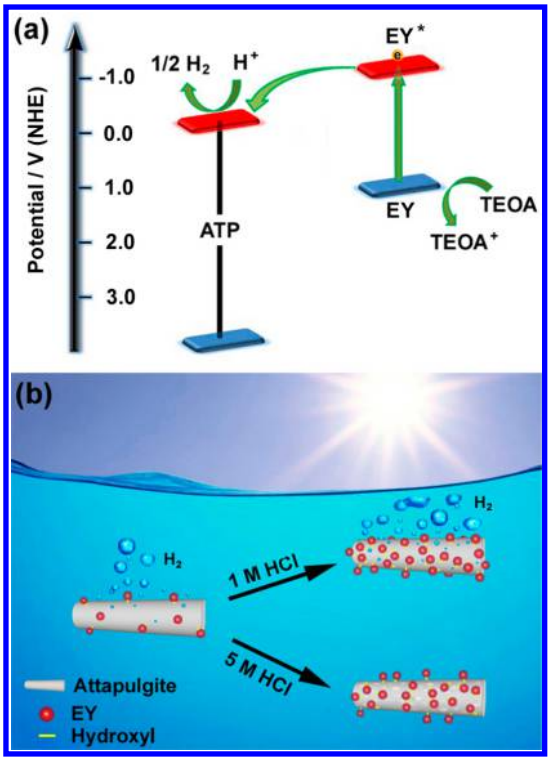

Figure 8. (a) Schematic illustration of charge separation and transfer over EY-ATP photocatalysts and (b) interface modified strategy of ATP we proposed under visible light ($\lambda \geq 420$ nm).

irradiation, electrons are excited from the HOMO to the LUMO of EY molecules; however, only electrons excited from the dye molecules adsorbed to the surface of ATP can transfer to ATP efficiently. Therefore, the surface hydroxyl activated sample (LCTATP) exhibited superb activity in comparison to the that of the original ATP due to the enhanced EY adsorption capacity. On the other hand, the sample treated with high concentration HCl (5 M) solution (HCTATP) with the activated surface shows inactivity due to the destruction of the M−OH tetrahedron (M = metallic elements) structures in ATP crystals. The proposed photocatalytic mechanism of the interface modification process of ATP is illustrated in Figure. 8b.

Photoelectrochemical (PEC) tests are often employed to research the behavior of photogenerated charge carriers in photocatalytic system.[55,56] An amperometric study of the ATP, HCTATP, and LCTATP electrodes coated on the ITO substrate were performed for five light on−off cycles under visible light illumination and were displayed in Figure 9a. As

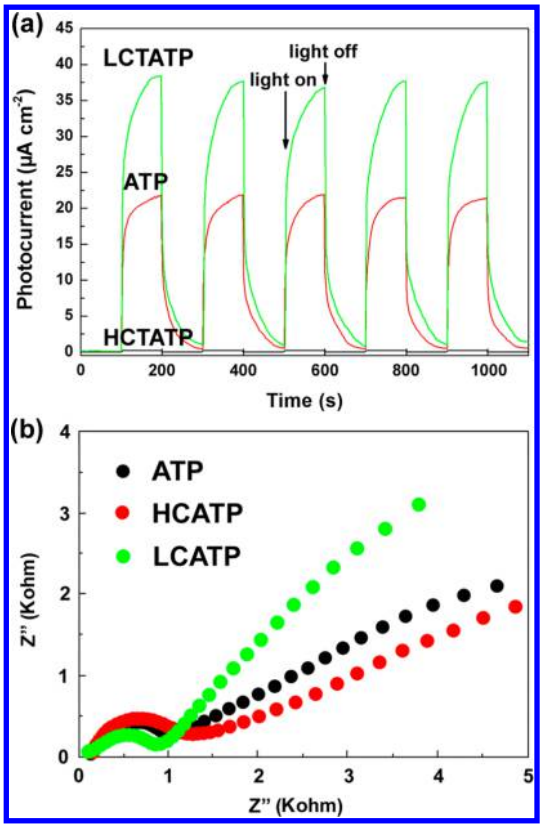

Figure 9. (a) Photocurrent density vs time for EY-sensitized ATP, HCTATP, and LCTATP coated on ITO glass in a mixed solution of Na_2SO_3 (0.35 M) and Na_2S (0.25 M) under visible light irradiation at 0.0 V using Ag/AgCl as a reference electrode and (b) EIS spectra of different samples.

expected, the LCTATP electrode exhibited a noticeable improvement in photocurrent intensity (38.2 μA cm^{-2}) compared to the other two samples. The insignificant photocurrent intensity (0.8 μA cm^{-2}) detected from curve HCTATP indicated that the crystal damage of the photocatalyst host matched well with the results of photocatalytic activity in Figure 7a. The photocatalysis and photoelectrochemical results were in good agreement with EIS data where obtained from the three samples as shown in Figure 9b. The representative EIS plots display an obvious decreased charge transfer resistance for LTCATP (852 Ω) compared to those of ATP (1093 Ω) and HTCATP (1258 Ω).

CONCLUSIONS

In summary, we have found a cheap and convenient route to hydrogen generation from water based on natural products under visible light irradiation. With the consideration of the interface properties and crystal structures of attapulgite (ATP), one of the important silicate minerals, the polarized photo-

DOI: 10.1021/acssuschemeng.6b00716
ACS Sustainable Chem. Eng. 2016, 4, 4601−4607

catalytic efficiency can be detected dramatically which coupled with Eosin Y (EY): low concentration HCl solution treated ATP (LCTATP) yielded a significantly enhanced hydrogen generation rate of 210 μmol h^{-1} with apparent quantum efficiency (QE) reaching 28.6% at 490 nm under visible light illumination; on the contrary, after being treated with high concentration HCl solution, the ATP (HCTATP) sample displayed insignificant activity (1.3 μmol h^{-1}) in the same catalytic system. We believe that this strategy will provide advancement for the utilization of natural silicate minerals in the water splitting applications under visible light.

AUTHOR INFORMATION

Corresponding Authors

* E-mail: iamxali@njupt.edu.cn. Phone: +86-02585866362.
*E-mail: iamwhuang@njupt.edu.cn.com.

Notes

The authors declare no competing financial interest.

ACKNOWLEDGMENTS

We acknowledge the financial support from the National Basic Research Program of China (2012CB933301, 2014CB648300), the Key Project of National High Technology Research of China (2011AA050526), the Ministry of Education of China (No. IRT1148), the National Synergetic Innovation Center for Advanced Materials (SICAM), the Natural Science Foundation of Jiangsu Province, China (BM2012010), the Project Funded by the Priority Academic Program Development of Jiangsu Higher Education Institutions (PAPD, YX03001), NUPTSF (Grant No. NY213103, NY214181, NY215077), and the National Natural Science Foundation of China (51172110, 51372119, 81273409, 61136003, 51272107, 61402240, 51572126).

REFERENCES

(1) Qu, Y.; Duan, X. Progress, Challenge and Perspective of Heterogeneous Photocatalysts. *Chem. Soc. Rev.* **2013**, *42*, 2568−2580.

(2) Chen, J.; Yang, H.; Miao, J.; Wang, H.; Liu, B. Thermodynamically Driven One-Dimensional Evolution of Anatase TiO_2 Nanorods: One-Step Hydrothermal Synthesis for Emerging Intrinsic Superiority of Dimensionality. *J. Am. Chem. Soc.* **2014**, *136*, 15310−15318.

(3) Fujishima, A.; Honda, K. Electrochemical Photolysis of Water at a Semiconductor Electrode. *Nature* **1972**, *238*, 37−38.

(4) Cummings, C. Y.; Marken, F.; Peter, L. M.; Wijayantha, K. G. U.; Tahir, A. A. New Insights into Water Splitting at Mesoporous a-Fe_2O_3 Films: A Study by Modulated Transmittance and Impedance Spectroscopies. *J. Am. Chem. Soc.* **2012**, *134*, 1228−1234.

(5) Yang, H.; Miao, J.; Hung, S.; Huo, F.; Chen, H.; Liu, B. Stable Quantum Dot Photoelectrolysis Cell for Unassisted Visible Light Solar Water Splitting. *ACS Nano* **2014**, *8*, 10403−10413.

(6) Moniz, S. J. A.; Shevlin, S. A.; Martin, D. J.; Guo, Z.; Tang, J. Visible-Light Driven Heterojunction Photocatalysts for Water Splitting−A Critical Review. *Energy Environ. Sci.* **2015**, *8*, 731−759.

(7) Zhang, J.; Wang, Q.; Wang, L.; Li, X.; Huang, W. Layer-Controllable WS_2-Reduced Graphene Oxide Hybrid Nanosheets with High Electrocatalytic Activity for Hydrogen Evolution. *Nanoscale* **2015**, *7*, 10391−10397.

(8) Zhang, X.; Liu, Y.; Kang, Z. 3D Branched ZnO Nanowire Arrays Decorated with Plasmonic Au Nanoparticles for High-Performance Photoelectrochemical Water Splitting. *ACS Appl. Mater. Interfaces* **2014**, *6*, 4480−4489.

(9) Gao, Y.; Zhang, L.; Ding, X.; Sun, L. Artificial Photosynthesis-Functional Devices for Light Driven Water Splitting with Photoactive Anodes Based on Molecular Catalysts. *Phys. Chem. Chem. Phys.* **2014**, *16*, 12008−12013.

(10) Kawashima, K.; Hojamberdiev, M.; Wagata, H.; Yubuta, K.; Vequizo, J. J. M.; Yamakata, A.; Oishi, S.; Domen, K.; Teshima, K. NH_3-Assisted Flux-Mediated Direct Growth of $LaTiO_2N$ Crystallites for Visible-Light-Induced Water Splitting. *J. Phys. Chem. C* **2015**, *119*, 15896−15904.

(11) Zou, Z.; Ye, J.; Sayama, K.; Arakawa, H. Direct Splitting of Water under Visible Light Irradiation with An Oxide Semiconductor Photocatalyst. *Nature* **2001**, *414*, 625−627.

(12) Li, J.; Liu, X.; Han, Q.; Yao, X.; Wang, X. Formation of WO_3 Nanotube-Based Bundles Directed by $NaHSO_4$ and Its Application in Water Treatment. *J. Mater. Chem. A* **2013**, *1*, 1246−1253.

(13) Lei, F.; Sun, Y.; Liu, K.; Gao, S.; Liang, L.; Pan, B.; Xie, Y. Oxygen Vacancies Confined in Ultrathin Indium Oxide Porous Sheets for Promoted Visible-Light Water Splitting. *J. Am. Chem. Soc.* **2014**, *136*, 6826−6829.

(14) Zhang, J.; Wang, L.; Liu, X.; Li, X.; Huang, W. High-Performance CdS/ZnS Core/Shell Nanorod Array Photoelectrode for Photoelectrochemical Hydrogen Generation. *J. Mater. Chem. A* **2015**, *3*, 535−541.

(15) Zhang, J.; Yu, J. G.; Zhang, Y. M.; Li, Q.; Gong, J. R. Visible Light Photocatalytic H_2-Production Activity of CuS/ZnS Porous Nanosheets Based on Photoinduced Interfacial Charge Transfer. *Nano Lett.* **2011**, *11*, 4774−4779.

(16) Tian, J.; Cheng, N.; Liu, Q.; Xing, W.; Sun, X. Cobalt Phosphide Nanowires: Efficient Nanostructures for Fluorescence Sensing of Biomolecules and Photocatalytic Evolution of Dihydrogen from Water under Visible Light. *Angew. Chem., Int. Ed.* **2015**, *54*, 5493−5497.

(17) Kang, Y.; Yang, Y.; Yin, L. C.; Kang, X.; Liu, G.; Cheng, H. M. An Amorphous Carbon Nitride Photocatalyst with Greatly Extended Visible-Light-Responsive Range for Photocatalytic Hydrogen Generation. *Adv. Mater.* **2015**, *27*, 4572−4577.

(18) Swierk, J. R.; Mallouk, T. E. Design and Development of Photoanodes for Water-Splitting Dye-Sensitized Photoelectrochemical Cells. *Chem. Soc. Rev.* **2013**, *42*, 2357−2387.

(19) Maeda, K.; Eguchi, M.; Youngblood, W. J.; Mallouk, T. E. Niobium Oxide Nanoscrolls as Building Blocks for Dye-Sensitized Hydrogen Production from Water under Visible Light Irradiation. *Chem. Mater.* **2008**, *20*, 6770−6778.

(20) Swierk, J. R.; McCool, N. S.; Mallouk, T. E. Dynamics of Electron Recombination and Transport in Water-Splitting Dye-Sensitized Photoanodes. *J. Phys. Chem. C* **2015**, *119*, 13858−13867.

(21) Gerischer, H. Electrochemical Techniques for the Study of Photosensitization. *Photochem. Photobiol.* **1972**, *16*, 243−260.

(22) Maeda, K.; Sahara, G.; Eguchi, M.; Ishitani, O. Hybrids of a Ruthenium (II) Polypyridyl Complex and a Metal Oxide Nanosheet for Dye-Sensitized Hydrogen Evolution with Visible Light: Effects of the Energy Structure on Photocatalytic Activity. *ACS Catal.* **2015**, *5*, 1700−1707.

(23) Youngblood, W. J.; Lee, S. H. A.; Maeda, K.; Mallouk, T. E. Visible Light Water Splitting Using Dye-Sensitized Oxide Semiconductors. *Acc. Chem. Res.* **2009**, *42*, 1966−1973.

(24) Zhang, X.; Veikko, U.; Mao, J.; Cai, P.; Peng, T. Visible-Light-Induced Photocatalytic Hydrogen Production over Binuclear RuII-Bipyridyl Dye-Sensitized TiO_2 without Noble Metal Loading. *Chem. - Eur. J.* **2012**, *18*, 12103−12111.

(25) Demas, J. N.; Taylor, D. G. On the "Intersystem Crossing" Yields in Ruthenium (II) and Osmium (II) Photosensitizers. *Inorg. Chem.* **1979**, *18*, 3177−3179.

(26) Swierk, J. R.; Méndez-Hernández, D. D.; McCool, N. S.; Liddell, P.; Terazono, Y.; Pahk, I.; Tomlin, J. J.; Oster, N. V.; Moore, T. A.; Moore, A. L.; Gust, D.; Mallouk, T. E. Metal-Free Organic Sensitizers for Use in Water-Splitting Dye-Sensitized Photoelectrochemical Cells. *Proc. Natl. Acad. Sci. U. S. A.* **2015**, *112*, 1681−1686.

(27) Le, T. T.; Akhtar, M. S.; Park, D. M.; Lee, J. C.; Yang, O.-B. Water Splitting on Rhodamine-B Dye Sensitized Co-Doped TiO_2 Catalyst under Visible Light. *Appl. Catal., B* **2012**, *111*, 397−401.

(28) Gurunathan, K.; Maruthamuthu, P.; Sastri, M. V. C. Photocatalytic Hydrogen Production by Dye-Sensitized Pt/SnO_2 and Pt/

DOI: 10.1021/acssuschemeng.6b00716
ACS Sustainable Chem. Eng. 2016, 4, 4601−4607

SnO_2/RuO_2 in Aqueous Methyl Viologen Solution. *Int. J. Hydrogen Energy* **1997**, *22*, 57−62.
(29) Nuraje, N.; Dang, X.; Qi, J.; Allen, M. A.; Lei, Y.; Belcher, A. M. Biotemplated Synthesis of Perovskite Nanomaterialsfor Solar Energy Conversion. *Adv. Mater.* **2012**, *24*, 2885−2889.
(30) Shimidzu, T.; Iyoda, T.; Koide, Y. An Advanced Visible-Light-Induced Water Reduct Ion with Dye-Sensitized Semiconductor Powder Catalyst. *J. Am. Chem. Soc.* **1985**, *107*, 35−41.
(31) Li, Y.; Guo, M.; Peng, S.; Lu, G.; Li, S. Formation of Multilayer-Eosin Y-Sensitized TiO_2 via Fe^{3+} Coupling for Efficient Visible-Light Photocatalytic Hydrogen Evolution. *Int. J. Hydrogen Energy* **2009**, *34*, 5629.
(32) Zhang, J.; Wang, W.; Liu, X. Ag-ZnO Hybrid Nanopyramids for High Visible-Light Photocatalytic Hydrogen Production Performance. *Mater. Lett.* **2013**, *110*, 204−207.
(33) Min, S.; Lu, G. Sites for High Efficient Photocatalytic Hydrogen Evolution on a Limited-Layered MoS_2 Cocatalyst Confined on Graphene Sheets-The Role of Graphene. *J. Phys. Chem. C* **2012**, *116*, 25415−25424.
(34) Li, Q.; Lu, G. Visible-Light Driven Photocatalytic Hydrogen Generation on Eosin Y-Sensitized Pt-Loaded Nanotube $Na_2Ti_2O_4(OH)_2$. *J. Mol. Catal. A: Chem.* **2007**, *266*, 75−79.
(35) Li, Q.; Jin, Z.; Peng, Z.; Li, Y.; Li, S.; Lu, G. High-Efficient Photocatalytic Hydrogen Evolution on Eosin Y-Sensitized Ti-MCM41 Zeolite under Visible-Light Irradiation. *J. Phys. Chem. C* **2007**, *111*, 8237−8241.
(36) Zhang, J.; Liu, X. Photocatalytic Hydrogen Production from Water under Visible Light Irradiation using A Dye-Sensitized Attapulgite Nanocrystal Photocatalyst. *Phys. Chem. Chem. Phys.* **2014**, *16*, 8655−8660.
(37) Zhang, J.; Liu, T.; Chen, R.; Liu, X. Vermiculite as a Natural Silicate Crystal for Hydrogen Generation from Photocatalytic Splitting of Water under Visible Light. *RSC Adv.* **2014**, *4*, 406−408.
(38) Zhang, J.; He, R.; Liu, X. Efficient Visible-Light Driven Photocatalytic Hydrogen Production from Water using Attapulgite Clay Sensitized by CdS Nanoparticles. *Nanotechnology* **2013**, *24*, 505401.
(39) Zhang, J.; Zhu, W.; Liu, X. Stable Hydrogen Generation from Vermiculite Sensitized by CdS Quantum Dot Photocatalytic Splitting of Water under Visible-Light Irradiation. *Dalton Trans.* **2014**, *43*, 9296−9302.
(40) Yang, H.; Tang, A.; Ouyang, J.; Li, M.; Mann, S. From Natural Attapulgite to Mesoporous Materials: Methodology, Characterization and Structural Evolution. *J. Phys. Chem. B* **2010**, *114*, 2390−2398.
(41) Liu, Y.; Kang, Y.; Mu, B.; Wang, A. Attapulgite/Bentonite Interactions for Methylene Blue Adsorption Characteristics from Aqueous Solution. *Chem. Eng. J.* **2014**, *237*, 403−410.
(42) Ma, J.; Zou, J.; Li, L.; Yao, C.; Kong, Y.; Cui, B.; Zhu, R.; Li, D. Nanocomposite of Attapulgite-Ag_3PO_4 for Orange II Photodegradation. *Appl. Catal., B* **2014**, *144*, 36−40.
(43) Mu, B.; Wang, A. One-Pot Fabrication of Multifunctional Superparamagnetic Attapulgite/Fe_3O_4/Polyaniline Nanocomposites Served as an Adsorbent and Catalyst Support. *J. Mater. Chem. A* **2015**, *3*, 281−289.
(44) Cui, E.; Lu, G. Modulating Photogenerated Electron Transfer and Hydrogen Production Rate by Controlling Surface Potential Energy on a Selectively Exposed Pt Facet on Pt/TiO_2 for Enhancing Hydrogen Production. *J. Phys. Chem. C* **2013**, *117*, 26415−26425.
(45) Min, S.; Lu, G. Enhanced Electron Transfer from the Excited Eosin Y to mpg-C_3N_4 for Highly Efficient Hydrogen Evolution under 550 nm Irradiation. *J. Phys. Chem. C* **2012**, *116*, 19644−19652.
(46) Min, S.; Lu, G. Sites for High Efficient Photocatalytic Hydrogen Evolution on a Limited-Layered MoS_2 Cocatalyst Confined on Graphene Sheets-The Role of Graphene. *J. Phys. Chem. C* **2012**, *116*, 25415−25424.
(47) Chen, L.; Liang, H.; Lu, Y.; Cui, C.; Yu, S. Synthesis of An Attapulgite Clay@Carbon Nanocomposite Adsorbent by a Hydrothermal Carbonization Process and Their Application in the Removal of Toxic Metal Ions from Water. *Langmuir* **2011**, *27*, 8998−9004.
(48) Xu, J.; Sun, Z.; Jia, L.; Li, B.; Zhao, L.; Liu, X.; Ma, Y.; Tian, H.; Wang, Q.; Liu, W.; Tang, Y. Visible Light Sensitized Attapulgite-Based Lanthanide Composites: Microstructure, Photophysical Behaviour and Biological Application. *Dalton Trans.* **2011**, *40*, 12909−12916.
(49) Valdes-aguilera, O.; Neckers, D. C. Aggregation Phenomena in Xanthene Dyes. *Acc. Chem. Res.* **1989**, *22*, 171−177.
(50) Zhang, X.; Jin, Z.; Li, Y.; Li, S.; Lu, G. Visible-Light-Induced Hydrogen Production over Pt-Eosin Y Catalysts with High Surface Area Silica Gel as Matrix. *J. Power Sources* **2007**, *166*, 74−79.
(51) Cai, Y.; Xue, J.; Polya, D. A Fourier Transform Infrared Spectroscopic Study of Mg-Rich, Mg-Poor and Acid Leached Palygorskites. *Spectrochim. Acta, Part A* **2007**, *66*, 282−288.
(52) Lai, S.; Yue, L.; Zhao, X.; Gao, L. Preparation of Silica Powder with High Whiteness from Palygorskite. *Appl. Clay Sci.* **2010**, *50*, 432−437.
(53) Gao, Y.; Ding, X.; Liu, J.; Wang, L.; Lu, Z.; Li, L.; Sun, L. Visible Light Driven Water Splitting in a Molecular Device with Unprecedentedly High Photocurrent Density. *J. Am. Chem. Soc.* **2013**, *135*, 4219−4222.
(54) Kong, C.; Min, S.; Lu, G. Dye-Sensitized NiS_x Catalyst Decorated on Graphene for Highly Efficient Reduction of Water to Hydrogen under Visible Light Irradiation. *ACS Catal.* **2014**, *4*, 2763−2769.
(55) Zhang, J.; Wang, Y.; Jin, J.; Zhang, J.; Lin, Z.; Huang, F.; Yu, J. Efficient Visible-Light Photocatalytic Hydrogen Evolution and Enhanced Photostability of Core/Shell CdS/g-C_3N_4 Nanowires. *ACS Appl. Mater. Interfaces* **2013**, *5*, 10317−10324.
(56) Guo, K.; Liu, Z.; Han, J.; Zhang, X.; Li, Y.; Hong, T.; Zhou, C. Higher-Efficiency Photoelectrochemical Electrodes of Titanium Dioxide-Based Nanoarrays Sensitized Simultaneously with Plasmonic Silver Nanoparticles and Multiple Metal Sulfides Photosensitizers. *J. Power Sources* **2015**, *285*, 185−194.

DOI: 10.1021/acssuschemeng.6b00716
ACS Sustainable Chem. Eng. 2016, 4, 4601−4607